論文 / 著書情報
Article / Book Information

Title	Persistent fluctuations in synchronization rate in globally coupled oscillators with periodic external forcing
Authors	Yu Atsumi, Hiroya Nakao
Citation	Physical Review E, Vol. 85, No. 5, pp. 056207
Pub. date	2012, 5
Journal URL	http://journals.aps.org/pre/
Copyright	Copyright (C) 2012 American Physical Society

Persistent fluctuations in synchronization rate in globally coupled oscillators with periodic external forcing

Yu Atsumi*
Department of Physics, Kyoto University, Kyoto 606-8502, Japan

Hiroya Nakao
Department of Mechanical and Environmental Informatics, Tokyo Institute of Technology, O-okayama 2-12, Meguro, Tokyo 152-8552, Japan

(Received 22 February 2012; published 14 May 2012)

A system of phase oscillators with repulsive global coupling and periodic external forcing undergoing asynchronous rotation is considered. The synchronization rate of the system can exhibit persistent fluctuations depending on parameters and initial phase distributions, and the amplitude of the fluctuations scales with the system size for uniformly random initial phase distributions. Using the Watanabe-Strogatz transformation that reduces the original system to low-dimensional macroscopic equations, we show that the fluctuations are collective dynamics of the system corresponding to low-dimensional trajectories of the reduced equations. It is argued that the amplitude of the fluctuations is determined by the inhomogeneity of the initial phase distribution, resulting in system-size scaling for the random case.

DOI: 10.1103/PhysRevE.85.056207 PACS number(s): 05.45.Xt

I. INTRODUCTION

Coupled oscillators have been analyzed as models of various real-world systems consisting of interacting dynamical elements, which display diverse types of rhythmic phenomena [1–16]. In particular, globally coupled oscillators have been intensively studied as the simplest model of systems exhibiting collective rhythms. A number of studies have shown that globally coupled oscillators converge to steady and stable synchronized states under appropriate conditions [1–3]. Globally coupled oscillators can also generate more complex behaviors [4–10]. For example, phase oscillators with global nonsinusoidal interaction can exhibit clustering behaviors, where the oscillators spontaneously split into several groups [4–7]. It is also known that globally coupled limit-cycle oscillators can split into clusters with differing amplitudes [8,9].

An interesting class of complex behaviors is nonstationary time-dependent collective dynamics [6–11]. For example, Han *et al*. reported that populations of Morris-Lecar neural oscillators with global coupling can repeat spontaneous synchronization and desynchronization, which are caused by the opposing effects of repulsive phase coupling along the limit cycle and the strong attraction of a fixed point inside the limit cycle [10]. Another interesting example is the slow switching dynamics of globally coupled phase oscillators, in which the system repeats spontaneous collapse and reorganization of clustered states due to heteroclinic connections in the phase space [6,7]. Nonstationary collective dynamics of coupled oscillators may be important in understanding transient behaviors of rhythmic systems [17,18], such as the spontaneous synchronization and desynchronization of collective rhythmic applause in concert halls [18].

In this study, we consider nonstationary asynchronous states in a system of phase oscillators with global repulsive coupling and periodic external forcing. We demonstrate that the phase distribution of the oscillators repeatedly contracts and expands as the oscillators rotate around the cycle when they are started from random initial conditions; this repeated contraction and expansion of the phase distribution results in persistent periodic (or chaotic) fluctuations in the synchronization rate. However, if the system starts from a "splay-state" initial condition in which the oscillators are equally allocated on the cycle, no fluctuation is observed in the synchronization rate. We determine a parameter region where such fluctuating dynamics occurs by numerical simulations and by linear stability analysis. Moreover, using the Watanabe-Strogatz transformation, we reduce the original high-dimensional model to a set of low-dimensional macroscopic equations and analyze its collective dynamics that corresponds to the fluctuations in the synchronization rate. We argue that the amplitude of the fluctuations is determined by inhomogeneity of the initial phase distributions, leading to system-size scaling behavior in the case of random initial conditions.

This paper is organized as follows. The model is introduced in Sec. II, and its dynamics are illustrated by numerical simulations in Sec. III. Section IV describes the linear stability analysis of the synchronized states. The Watanabe-Strogatz transformation is introduced in Sec. V, and the dynamics of the reduced equations is shown in Sec. VI. The effect of the inhomogeneous initial conditions and the system-size scaling behavior are considered in Sec. VII, and the study is summarized in Sec. VIII.

II. MODEL

We consider the following equation to represent the model of globally coupled phase oscillators with sinusoidal interaction that are subjected to periodic external forcing:

$$\dot{\theta}_j = \omega + \frac{\epsilon}{N}\sum_{n=1}^{N}\cos(\theta_n - \theta_j - \delta) + k\cos(\Omega t - \theta_j), \quad (1)$$

for $j = 1, \ldots, N$, where N is the number of oscillators, θ_j is the phase of the jth oscillator, and ω is the intrinsic frequency

*atsumi@scphys.kyoto-u.ac.jp

common to all the oscillators. The second term on the right-hand side represents global coupling between the oscillators, where ϵ is the coupling strength and $\delta \in (-\pi,\pi]$ gives the phase shift of the coupling. The third term represents the periodic external forcing, whose intensity is k and frequency is Ω. This model is a simple variant of the classical Kuramoto model [1,19,20] with an additional periodic external forcing and without frequency inhomogeneity. It can be derived from the models of globally coupled limit-cycle oscillators that are subjected to periodic forcing by the phase reduction method under appropriate assumptions and approximations [1].

Phase oscillator models similar to Eq. (1) have been widely studied in the past. For example, Sakaguchi [21] considered globally coupled phase oscillators with distributed frequencies under periodic external forcing and revealed the existence of two types of synchronized states, namely, the forced-entrainment state (which we will call the locked state) and the mutual-entrainment state (the synchronized drifting state). More recently, Childs and Strogatz [22] gave a detailed bifurcation analysis of a similar model with frequency distribution using the Ott-Antonsen ansatz [23], which is a powerful method that can reduce the original high-dimensional system to a simple two-dimensional dynamical system. The simple model given by Eq. (1) may be adapted to describe the synchronization of heart cell aggregates with external forcing [24] or the pathological synchronization in Parkinson's disease with deep-brain stimulation treatment [25,26]. In the present study, we investigate the nonstationary asynchronous states of Eq. (1) with repulsive coupling. We focus on the fluctuations in the synchronization rate and analyze their dependence on initial conditions and on the system size.

The interaction term in Eq. (1) gives in-phase attractive coupling when $\epsilon \sin\delta > 0$ and antiphase repulsive coupling when $\epsilon \sin\delta < 0$ ($\delta = 0$ corresponds to a singular case wherein the system is completely integrable [27]; we do not consider this case). The external forcing term tends to entrain the oscillators and provides a facilitating effect for synchronization. Introducing a rotating reference frame with an angular velocity Ω by redefining the phase variables as $\theta_j \to \theta_j + \Omega t$ and rescaling the time t as well as the parameters ϵ and k, we can transform Eq. (1) to

$$\dot{\theta_j} = 1 + \frac{\epsilon}{N}\sum_{n=1}^{N}\cos(\theta_n - \theta_j - \delta) + k\cos\theta_j, \qquad (2)$$

for $j = 1,\ldots,N$. We analyze this rescaled autonomous equation in the following sections. It should be noted that the transformed equation (2) is formally equivalent to an equation for a system of globally coupled active rotators without external forcing [28].

To measure the degree of synchrony, we use the complex order parameter [1]

$$W = Re^{i\Xi} = \frac{1}{N}\sum_{n=1}^{N} e^{i\theta_n}, \qquad (3)$$

where R and Ξ take values in $[0,1]$ and $[0,2\pi)$, respectively. Larger values of R indicate higher coherence; $R = 0$ corresponds to a completely incoherent state, and $R = 1$ corresponds to a completely synchronized state. This R is

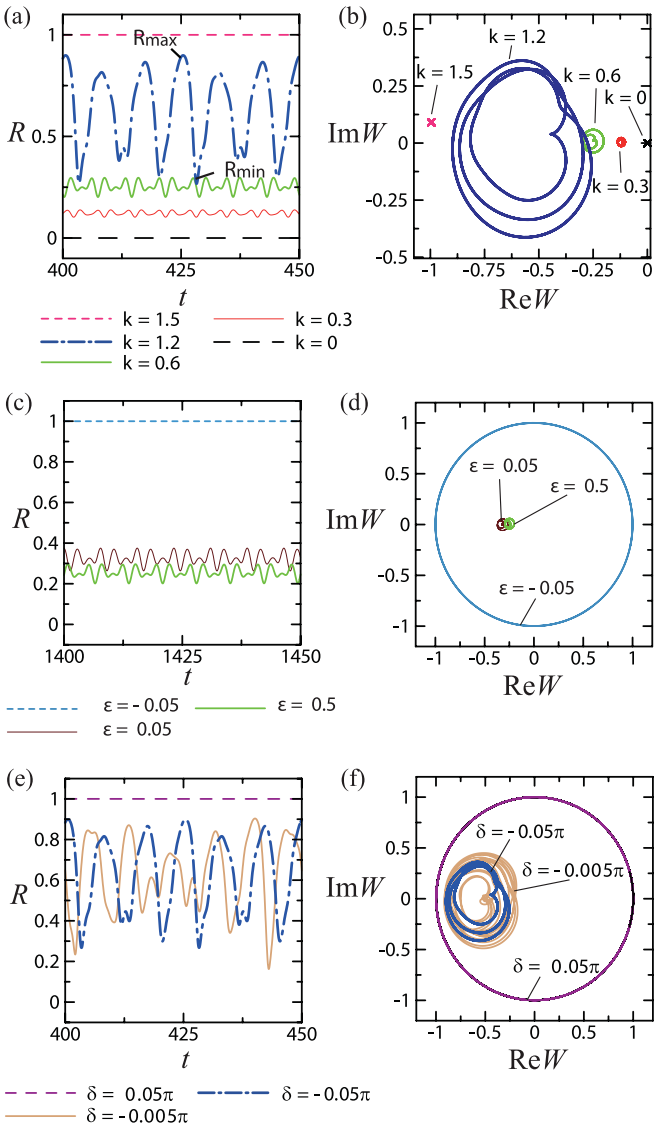

FIG. 1. (Color online) Asynchronous fluctuating states of the oscillators started from random initial conditions. $N = 20$ oscillators are used. Time sequences of the synchronization rate R are plotted in (a), (c), and (e), and the corresponding trajectories of the order parameter $W = Re^{i\Xi}$ on the complex plane are plotted in (b), (d), and (f). (a), (b) External forcing intensity k is varied ($0 \leqslant k \leqslant 1.5$) while coupling strength $\epsilon = 0.5$ and coupling phase shift $\delta = -0.05\pi$ are fixed. (c), (d) ϵ is varied ($\epsilon = -0.05, 0.05, 0.5$) while $k = 0.6$ and $\delta = -0.05\pi$ are fixed. (e), (f) δ is varied ($\delta = -0.05\pi, -0.005\pi, 0.05\pi$) while $k = 1.2$ and $\epsilon = 0.5$ are fixed.

referred to as the synchronization rate. As can be seen in the subsequent sections, R can exhibit nonstationary fluctuations (see Fig. 1). We thus define the amplitude of the fluctuations ΔR as the difference between the maximum value $R_{\max}$ and minimum value $R_{\min}$ of the time sequence of R, i.e., $\Delta R = R_{\max} - R_{\min}$, sufficiently after the initial transient of the system has passed.

III. NUMERICAL SIMULATIONS

First, we illustrate the typical behaviors of the system by numerical simulations. The completely synchronized state

with $R = 1$ can evidently be classified into two types [21]. The first type corresponds to the complete phase locking of all the oscillators to the periodic external forcing, which occurs at a sufficiently large $|k|$ whether coupling is attractive or repulsive. In this case, all the phase variables $\{\theta_j(t)\}$ take the same constant value. We refer to this state as the "locked state." The second type of complete synchronization is that caused by attractive coupling. The oscillators exhibit synchronized drift, where all $\{\theta_j\}$ monotonously increase while maintaining completely synchrony. This occurs when the coupling is attractive, i.e., $\epsilon \sin\delta > 0$, and when the external forcing $|k|$ is not sufficiently large to entrain the oscillators. We refer to this state as the "synchronized drifting state." If neither of these completely synchronized states is possible, the oscillators exhibit asynchronous rotations around the cycle and their distribution can repeatedly contract and expand. As can be seen in the subsequent sections, the dynamics in the asynchronous state largely differs depending on the initial conditions of the individual oscillators. We refer to this dynamical regime as the "asynchronous state." (We use this term in a nonstandard way to represent the dynamical regime where R takes neither 0 nor 1 but fluctuates in between them.)

A. Random initial conditions

Figures 1 and 2 show the dynamics of the system obtained by direct numerical simulations of Eq. (2) using $N = 20$ oscillators. The initial phase values $\{\theta_j(t = 0)\}$ are selected randomly and independently from a uniform distribution in $[0,2\pi)$, except Fig. 2(d) for which the splay-state initial distribution (explained later) is used. In this case, the dynamics of the oscillators in the asynchronous state fluctuates as described below.

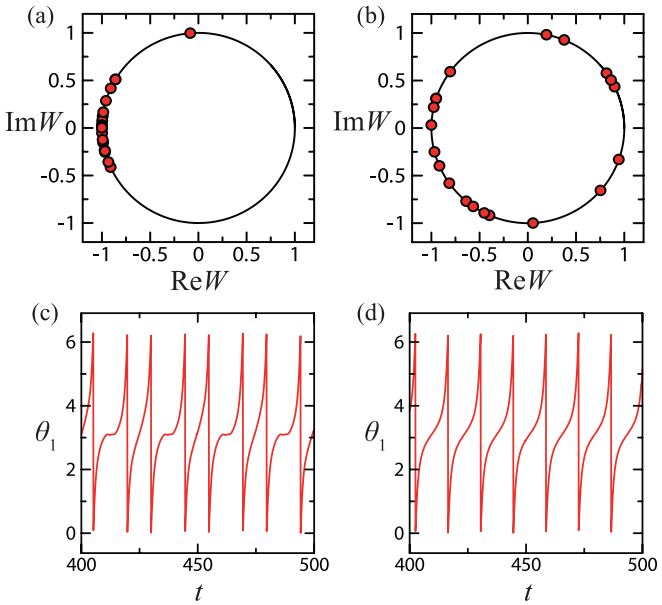

FIG. 2. (Color online) Dynamics of the oscillators in the asynchronous fluctuating state. The number of oscillators is $N = 20$ and the parameters are $k = 1.2$, $\epsilon = 0.5$, and $\delta = -0.05\pi$. The initial distribution of the oscillators is uniformly random in (a)–(c), and is a splay state in (d). (a), (b) Snapshots of the oscillators on the cycle for the random initial condition. The oscillator distribution repeatedly contracts (a) and expands (b). (c), (d) Typical time sequences of the phase of a single oscillator ($i = 1$). For the random initial condition, alternant fluctuations are observed in the oscillations (c), whereas for the splay-state initial condition, no fluctuation is observed (d).

Figures 1(a), 1(c), and 1(e) shows the time sequences of R, and Figs. 1(b), 1(d), and 1(f) plots the dynamics of $W = Re^{i\Xi}$ on the complex plane for differing values of k, ϵ, and δ, respectively. In Figs. 1(a) and 1(b), k is varied while $\epsilon = 0.5$ and $\delta = -0.05\pi$ are fixed. At $k = 0$, the external forcing is absent and the oscillators are completely desynchronized, which yields $R = 0$. At $k = 1.5$, all the oscillators are entrained to the external forcing, yielding $R = 1$. In either case, W is fixed on the complex plane and is stationary. For intermediate values of k, R exhibits persistent fluctuations. The amplitude and baseline (average) of the oscillations increase with k until the system becomes completely entrained. The corresponding trajectories of W on the complex plane are rather complicated but closed, i.e., the fluctuations are periodic in this case (the observed fluctuations are mostly periodic but can also be chaotic at small δ depending on initial conditions).

Similarly, Figs. 1(c) and 1(d) show the dynamics of the system for several values of ϵ with fixed values of $k = 0.6$ and $\delta = -0.05\pi$. R exhibits periodic fluctuations when the coupling is repulsive ($\epsilon = 0.05$ or $\epsilon = 0.5$). When the coupling is attractive ($\epsilon = -0.05$), all the oscillators become completely synchronized and R simply converges to 1. W simply rotates along the full circle $|W| = 1$ on the complex plane. Figures 1(e) and 1(f) show the dynamics of the system for several values of δ with fixed values of $k = 1.2$ and $\epsilon = 0.5$. R fluctuates only when the coupling is repulsive ($\delta < 0$). For the particular realization of the initial condition used here, the fluctuations are periodic when $\delta = -0.05\pi$ and is chaotic when $\delta = -0.005\pi$ (with the maximum Lyapunov exponent 0.112). When the coupling is attractive ($\delta > 0$), all the oscillators become completely synchronized without fluctuations, yielding $R = 1$.

Figures 2(a) and 2(b) show typical snapshots of the oscillators on their cycle observed at $R = R_{\max}$ and $R = R_{\min}$ for $k = 1.2$, $\epsilon = 0.5$, and $\delta = -0.05\pi$ plotted in Fig. 1(a). We observe that the distribution of the oscillators repeatedly contracts (a) or expands (b). The dynamics of a single oscillator phase in this situation is shown in Fig. 2(c). Reflecting the periodic fluctuations of all oscillators, we can observe that each oscillator undergoes periodically modulated rotations, i.e., the time required for the oscillator to perform one rotation around the cycle exhibits long-short alternations. If we use the splay-state initial condition instead of the random initial condition, no such alternation is observed [Fig. 2(d)] as we explain in the next section.

B. Splay-state initial condition

The numerical results shown in Fig. 1 are obtained for random initial phase distributions. Here, instead of the random distribution, we consider the splay-state initial distribution [27,28], which is given by equally spaced initial allocations of the phase variables $\{\theta_j(0)\}$ in $[0,2\pi)$, i.e., $\theta_j(0) = 2\pi j/N$ ($j = 1, \ldots, N$). It is known that this particular homogeneous distribution of oscillators is significant for the dynamics of the system [27,28]. If the coupling is attractive, $\epsilon \sin\delta > 0$, or if

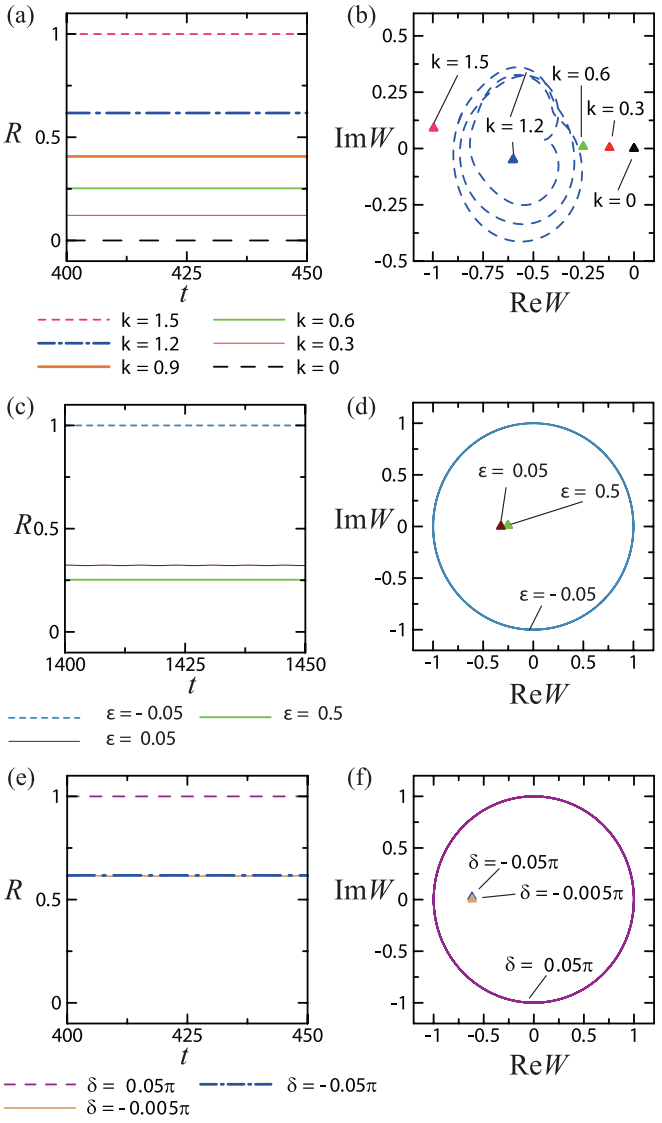

FIG. 3. (Color online) Absence of fluctuations in the asynchronous state started from splay-state initial conditions. $N = 20$ oscillators are used. Time sequences of the synchronization rate R are plotted in (a), (c), and (e), and the corresponding trajectories of the order parameter $W = Re^{i\Theta}$ on the complex plane are plotted in (b), (d), and (f). The parameters are the same as those used in Figs. 1(a) and 1(b). External forcing intensity k is varied while coupling strength $\epsilon = 0.5$ and coupling phase shift $\delta = -0.05\pi$ are fixed. (c), (d) ϵ is varied while $k = 0.6$ and $\delta = -0.05\pi$ are fixed. (e), (f) δ is varied while $k = 1.2$ and $\epsilon = 0.5$ are fixed. The trajectory of W at $k = 1.2$ observed for the random initial condition is also plotted in (b) for comparison.

the external forcing k is sufficiently strong, the dynamics of the system after the initial transient is identical to that under random initial conditions, i.e., the system converges to either of the completely synchronized states. However, if the coupling is repulsive and the parameter values are in the regime of asynchronous fluctuating state for random initial conditions with intermediate values of k, the dynamics of the system can be very different.

Figures 3(a), 3(c), and 3(e) plot the time sequences of R, and Figs. 3(b), 3(d), and 3(f) plot the dynamics of W on the complex plane using the same sets of parameter values of k, ϵ, and δ as those used for Fig. 1. In sharp contrast to the previous case with random initial conditions, even if the parameters are in the asynchronous state, R does not fluctuate but converges to nearly constant values between $R = 0$ and $R = 1$, which is close to the corresponding baselines of periodic fluctuations in the random case. W is nearly fixed on the complex plane and merely changes its location depending on the parameter values as shown in Figs. 3(b), 3(d), and 3(f). In fact, R fluctuates when N is finite; however, the fluctuation is negligible. For example, with $N = 20$ for Fig. 3, ΔR is merely $O(10^{-3})$ and is even smaller for larger N. For comparison, the trajectory observed under the random initial condition at $k = 1.2$, $\epsilon = 0.5$, and $\delta = -0.05\pi$ is also plotted in Fig. 3(b).

C. Effect of initial inhomogeneity

The above results indicate that the initial phase distribution, presumably its inhomogeneity, is essential for the fluctuations. Therefore we consider perturbed splay-state initial conditions, in addition to the random initial conditions, and examine the dependence of the dynamics on N.

First, we consider a situation wherein only a single oscillator is perturbed from the splay state; that is, we prepare a splay state and shift the initial phase θ_1 of the oscillator $j = 1$ by a small constant $a > 0$. All the other $N - 1$ oscillators are kept unchanged. Figure 4(a) plots the time sequences of R for several values of the initial phase shift a. The system size is $N = 20$, and the parameter values are $k = 1.2$, $\epsilon = 0.5$, and $\delta = -0.05\pi$. We observe that R exhibits oscillatory fluctuations when $a > 0$. $R_{\max}$ and $R_{\min}$ sufficiently after the initial transient are plotted in Fig. 4(b), which shows that the fluctuations become larger as a is increased. In Fig. 4(c), ΔR is plotted against a. We can observe that ΔR increases approximately linearly with a for small a. Similarly, Fig. 4(d) shows the time sequences of R for differing values of N, Fig. 4(e) plots $R_{\max}$ and $R_{\min}$ against N, and Fig. 4(f) plots ΔR against $1/N$ with fixed $a = 0.1$. We observe that ΔR is inversely proportional to N, and R converges to a constant value as N becomes large.

Next, we consider a situation wherein multiple initial phases are simultaneously shifted; that is, we prepare a splay state and shift the first M oscillator phases $j = 1, \ldots, M$ by a fixed amount a. For example, Fig. 5(a) shows the dependence of ΔR on a with $N = 1000$ and $M = 50$ for $k = 1.2$ and $k = 0.6$. ΔR increases linearly with a for small a, as in the previous case. Figure 5(b) plots ΔR against M with $N = 1000$ and $a = 0.1$. It can be observed that ΔR increases linearly with M for small M. The dependence of ΔR on $1/N$ is plotted in Fig. 5(c) when $M = 50$. As in the previous case, ΔR is inversely proportional to N for large N. Finally, Fig. 5(d) shows the dependence of ΔR on N when the ratio of the shifted oscillators to the total oscillators M/N is kept constant. We now observe that ΔR exhibits negligible dependence on N, in contrast to the previous case. These results suggest that the degree of initial inhomogeneity is indeed the cause of the fluctuations.

Now, we reconsider the random initial conditions. When N is sufficiently large, the initial phases of the oscillators would nearly be homogeneously distributed in $[0, 2\pi)$ and the random initial conditions would effectively be similar to the

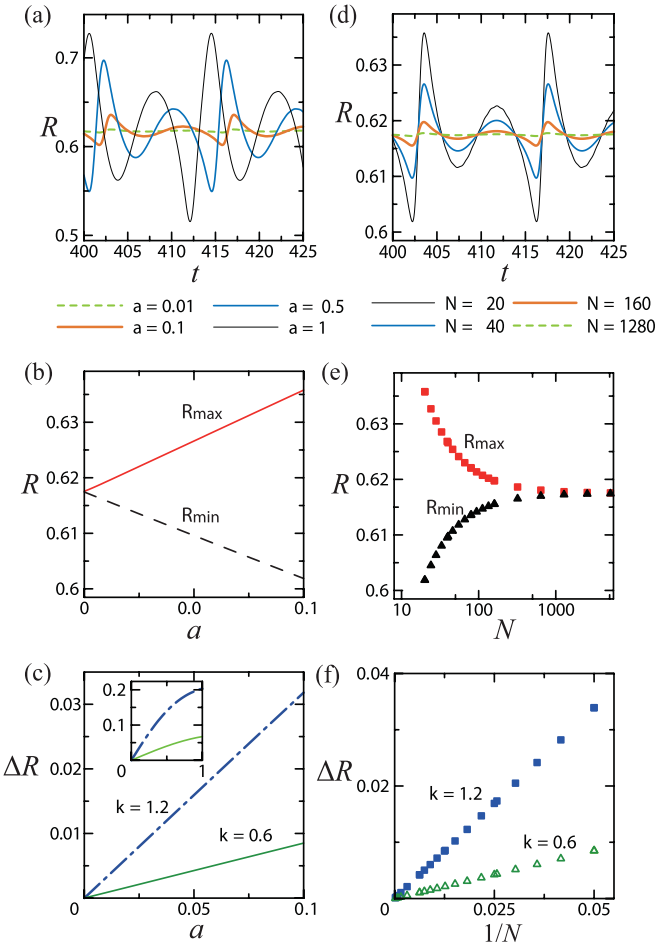

FIG. 4. (Color online) Dependence of the synchronization rate R on the small phase shift a from the splay state and on the system size N. Parameter values are $k = 1.2$ or $k = 0.6$, $\epsilon = 0.5$, and $\delta = -0.05\pi$. (a) Time sequences of R for different values of a at $k = 1.2$. (b) Dependence of the maximum value $R_{\max}$ and the minimum value $R_{\min}$ of R on a at $k = 1.2$. (c) Amplitude of the fluctuations $\Delta R = R_{\max} - R_{\min}$ vs a at $k = 0.6$ and $k = 1.2$. (d) Time sequences of R on N with $a = 0.1$ and $k = 1.2$. (e) Dependence of $R_{\max}$ and $R_{\min}$ on N with $a = 0.1$ and $k = 1.2$. (f) ΔR vs the inverse system size $1/N$ at $k = 0.6$ and $k = 1.2$ with $a = 0.1$.

splay-state initial condition. Therefore we expect that ΔR decreases with N, because the inhomogeneity of the system statistically decreases with N. This is confirmed in Fig. 6. Figure 6(a) plots R against N and Fig. 6(b) shows ΔR vs $1/N$ for $k = 1.2$, $\epsilon = 0.5$, and $\delta = -0.05\pi$. Results obtained for 30 random initial conditions are simultaneously plotted. As we increase N, R converges to a common fixed value independent of the initial randomness. ΔR decreases and eventually converges to 0.

These results indicate that ΔR is an increasing function of the overall inhomogeneity added to the splay state. The reason for the dependence of ΔR on N is discussed in Sec. VII.

D. Phase diagrams

Here we examine the dependence of the overall behavior of the system on the parameters ϵ,k, and δ. Figure 7 shows the phase diagrams on the ϵ-k plane obtained by direct numerical

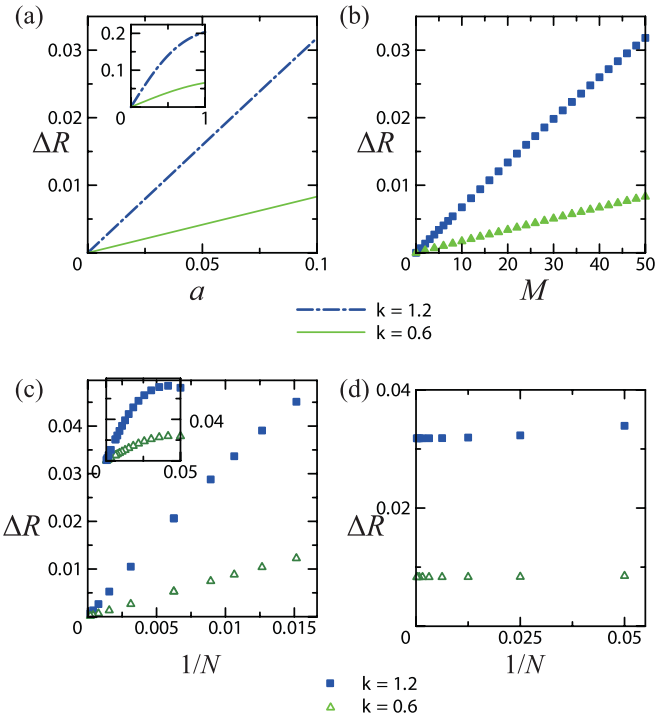

FIG. 5. (Color online) Dependence of the amplitude of fluctuations ΔR on the initial shift a, the total number of oscillators N, and the number of oscillators that are shifted initially M. (a) ΔR vs a when a fixed number of oscillators ($M = 50$) is simultaneously shifted. The total number of oscillators is $N = 1000$. (b) ΔR vs M for a fixed phase shift $a = 0.1$. The total number of oscillators is $N = 1000$. (c) ΔR vs $1/N$ when the a fixed number ($M = 5$) of oscillators is simultaneously shifted by a fixed amount $a = 0.1$. (d) ΔR vs $1/N$ when a fixed proportion ($M/N = 5\%$) of oscillators is simultaneously shifted by a fixed amount $a = 0.1$. The parameters are fixed at $\delta = -0.05\pi$ and $\epsilon = 0.5$.

simulations of Eq. (2) for several values of δ. We use $N = 20$ oscillators with uniformly random initial phases in $[0,2\pi)$. We classify the dynamics into three regimes, namely, the locked, synchronized drifting, and asynchronous states, by examining the time sequences of the order parameter. In each phase diagram, we observe a wide region of repulsive coupling

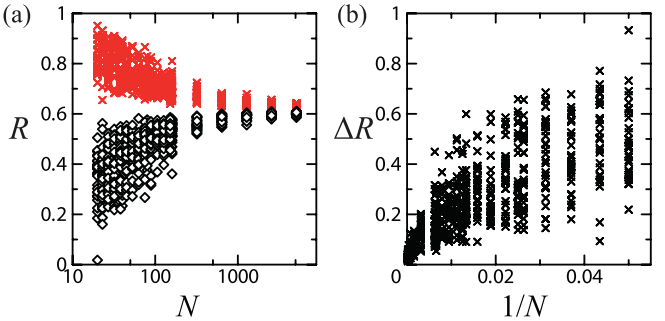

FIG. 6. (Color online) Dependence of the synchronization rate R and the amplitude of fluctuations ΔR on the number of oscillators N obtained for 30 different random initial conditions. Parameter values are $k = 1.2$, $\epsilon = 0.5$, and $\delta = -0.05\pi$. (a) Dependence of the maximum value $R_{\max}$ and the minimum value $R_{\min}$ of R on the number of oscillators N. (b) ΔR vs $1/N$.

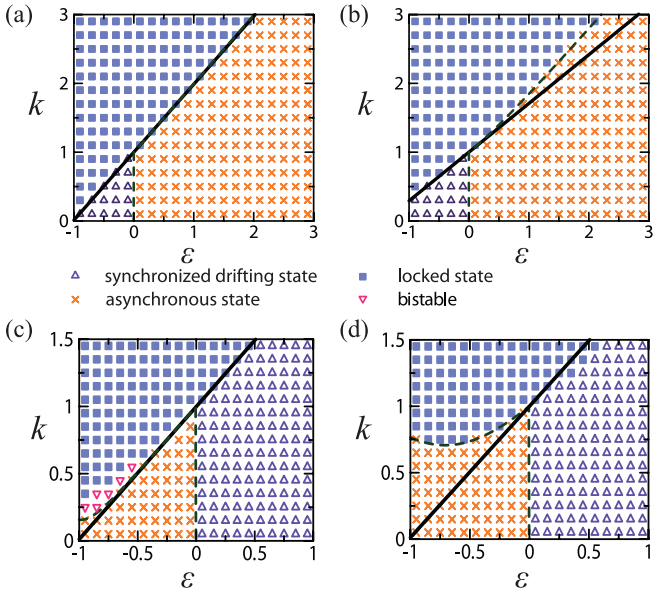

FIG. 7. (Color online) Phase diagrams on the ϵ-k plane obtained by numerical simulations with $N = 20$ oscillators at (a) $\delta = -0.05\pi$, (b) $\delta = -0.25\pi$, (c) $\delta = 0.05\pi$, and (d) $\delta = 0.25\pi$. The initial phases of the oscillators are selected randomly from a uniform distribution in $[0,2\pi)$. In (c), a small region exists where both the locked and asynchronous states are observed depending on the initial conditions.

where the oscillators rotate asynchronously around the cycle and the synchronization rate fluctuates. The asynchronous state and the two completely synchronized states (locked and synchronized drifting) are mutually exclusive in most cases, except for small bistable regions where both the locked and the synchronized drifting states are both possible depending on initial conditions. The same phase diagram is also obtained by starting from splay-state initial conditions and examining if R, which asymptotically becomes almost constant in this case, converges to some intermediate values between 0 and 1.

IV. LINEAR STABILITY ANALYSIS

In this section, we examine the conditions for the linear stability of the two completely synchronized states, namely, the locked state and the synchronized drifting state. First, let us consider the existence condition. When the system is completely synchronized, all phases $\{\theta_j\}$ are of the same value $\bar{\theta}$. Substituting $\theta_1 = \theta_2 = \cdots = \theta_N = \bar{\theta}$ in Eq. (2), we can obtain the evolution equation for $\bar{\theta}$ as

$$\dot{\bar{\theta}}(t) = 1 + \epsilon \cos\delta + k \cos\bar{\theta}. \tag{4}$$

When $|k| > 1 + \epsilon \cos\delta$, Eq. (4) has fixed points that satisfy $k \cos\bar{\theta} = -(1 + \epsilon \cos\delta)$. There are two solutions in $[0,2\pi)$, and only one of them is stable under the dynamics given by Eq. (4). Therefore we denote this stable fixed point by θ^*, which corresponds to the locked state. Obviously, the stability of the solution $\bar{\theta}(t) = \theta^*$ under Eq. (4) does not necessarily indicate the stability of the locked solution $\theta_1 = \theta_2 = \cdots = \theta_N = \theta^*$ of the full system, given by Eq. (2). When $|k| < 1 + \epsilon \cos\delta$, Eq. (4) cannot possess fixed points and $\bar{\theta}(t)$ exhibits an oscillatory increase with time. Therefore the border between the locked and synchronized drifting solutions is given by

$$k = 1 + \epsilon \cos\delta. \tag{5}$$

Next, we consider the linear stability of the locked solution, $\theta_1 = \theta_2 = \cdots = \theta_N \equiv \theta^*$. Solving the characteristic equation for the Jacobian matrix of the linearized equation of Eq. (2) around this fixed point, we obtain one eigenvalue $\lambda_1 = -\epsilon \sin\delta$ and $N-1$ degenerate eigenvalues $\lambda_{2,\ldots,N} = -\epsilon \sin\delta - k \sin\theta^*$. Therefore the conditions for the locked solution to be linearly stable, i.e., for the eigenvalues to be negative, are given by

$$\epsilon \sin\delta > 0, \tag{6}$$

and

$$\epsilon^2 + 2\epsilon \cos\delta + 1 < k^2. \tag{7}$$

The critical value k_c of k at which the locked state loses stability is given by $k_c^2 = \epsilon^2 + 2\epsilon \cos\delta + 1$.

Now, to analyze the linear stability of the synchronized drifting solution, $\theta_1 = \theta_2 = \cdots = \theta_N \equiv \bar{\theta}(t)$, we calculate the averaged growth rates of small perturbations given to Eq. (2) over one period of $\bar{\theta}(t)$, namely, the Floquet exponents $\tilde{\lambda}_{1,\ldots,N}$. It can be shown that the eigenvectors do not depend on time, so the Floquet exponents can easily be calculated as

$$\tilde{\lambda}_1 = 0, \tag{8}$$

and

$$\tilde{\lambda}_{2,\ldots,N} = -\epsilon \sin\delta \int_0^{2\pi} \frac{d\bar{\theta}}{1 + \epsilon \cos\delta + k \cos\bar{\theta}}, \tag{9}$$

where the zero eigenvalue $\tilde{\lambda}_1$ results from the time-translational symmetry of the dynamics. The integral on the right-hand side in Eq. (9) is positive whenever the synchronized drifting solution exists, i.e., $|k| < 1 + \epsilon \cos\delta$. Therefore the linear stability condition is simply given by

$$\epsilon \sin\delta > 0; \tag{10}$$

namely, it is solely determined by the global coupling term and is independent of k.

The existence condition Eq. (5) and the linear stability conditions Eqs. (6), (7), and (10) are drawn in the phase diagrams in Fig. 7, which explains the borders between different dynamical states well, i.e., the phase diagrams can be understood within the linear stability analysis of the synchronized states. However, as we already discussed in Sec. III, the dynamics in the asynchronous state largely differs depending on the initial conditions and nonstationary fluctuations are observed in the synchronization rate; the amplitude of these fluctuations depends on the initial inhomogeneity. In the following sections, we analyze such fluctuations in more detail.

V. WATANABE-STROGATZ TRANSFORMATION

Since the system consists of N oscillators and therefore has a high-dimensional phase space, it is difficult to observe the full trajectories and analyze them. Therefore we use the Watanabe-Strogatz transformation [27–30], which is a powerful method applicable to a class of globally coupled dynamical systems including Eq. (2). It transforms the dynamical variables of the system from N phase variables to three macroscopic

dynamical variables with $N-3$ constants of motion, thereby drastically reducing the degree of freedom and making the analysis much easier.

In Refs. [27,28], Watanabe and Strogatz proved that an N-dimensional system of the form

$$\dot{\theta}_j(t) = f + g\cos\theta_j + h\sin\theta_j \tag{11}$$

with $j = 1,\ldots,N$ can be reduced to a low-dimensional system of three essential macroscopic variables. Here, $f(\theta_1,\ldots,\theta_N,t)$, $g(\theta_1,\ldots,\theta_N,t)$, and $h(\theta_1,\ldots,\theta_N,t)$ are 2π-periodic with respect to each θ_k $(k = 1,\ldots,N)$. Equation (11) obviously includes Eq. (2) with the functions f, g, and h given by

$$f = 1, \quad g = \frac{1}{N}\sum_{j=1}^{N}\cos(\theta_j - \delta) + k, \qquad h = \frac{1}{N}\sum_{j=1}^{N}\sin(\theta_j - \delta). \tag{12}$$

The Watanabe-Strogatz (WS) transformation is given by the following change of the phase variables $\{\theta_j\}$ to new variables γ, Θ, Ψ, and $\{\psi_j\}$ $(j = 1,\ldots,N)$:

$$\tan\frac{\theta_j(t)-\Theta(t)}{2} = \sqrt{\frac{1+\gamma(t)}{1-\gamma(t)}}\tan\frac{\psi_j-\Psi(t)}{2}, \tag{13}$$

where γ, Θ, and Ψ are the three macroscopic variables. It can then be shown that the new variables $\{\psi_j\}$ $(j = 1,\ldots,N)$ are in fact constants of motion, provided that the macroscopic variables γ, Θ, and Ψ satisfy appropriate evolution equations given below. The original N phase variables $\{\theta_j(t)\}$ are converted to the N constants $\{\psi_j\}$ and to the three macroscopic variables γ, Θ, and Ψ that contain all the information of the system dynamics. The dynamics of the system described by Eq. (11) is restricted on a three-dimensional manifold specified by the constants of motion $\{\psi_j\}$, which are determined by the initial conditions of the system.

The evolution equations of the three macroscopic variables in the present case can explicitly be written as follows [27,28]:

$$\begin{aligned}\dot{\gamma}(t) &= -(1-\gamma^2)(g\sin\Theta - h\cos\Theta),\\ \dot{\Theta}(t) &= 1 - \frac{1}{\gamma}(g\cos\Theta + h\sin\Theta),\\ \dot{\Psi}(t) &= -\frac{\sqrt{1-\gamma^2}}{\gamma}(g\cos\Theta + h\sin\Theta),\end{aligned} \tag{14}$$

where the functions g and h are given in Eq. (12). They can be expressed using γ, Θ, and Φ as

$$\begin{aligned} g &= -\epsilon\{P\cos(\Theta-\delta) + Q\sin(\Theta-\delta)\} + k,\\ h &= -\epsilon\{P\sin(\Theta-\delta) - Q\cos(\Theta-\delta)\},\end{aligned} \tag{15}$$

where P and Q are global fields of the system defined by

$$P = \frac{1}{N}\sum_{j=1}^{N}F(\psi_j-\Psi), \quad Q = \frac{1}{N}\sum_{j=1}^{N}G(\psi_j-\Psi). \tag{16}$$

Here, the functions F and G are defined to be $F(\psi_j-\Psi) = -\cos(\theta_j-\Theta)$ and $G(\psi_j-\Psi) = \sin(\theta_j-\Theta)$, and are explicitly given from Eq. (13) as [28]

$$F(\psi) = \frac{\gamma-\cos\psi}{1-\gamma\cos\psi}, \quad G(\psi) = \frac{\sqrt{1-\gamma^2}\sin\psi}{1-\gamma\cos\psi}. \tag{17}$$

The phase space of γ, Θ, and Ψ contains a singular point at $\gamma = 0$. To avoid this singularity, Cartesian-type coordinates $x = \gamma\cos\Theta$, $y = \gamma\sin\Theta$, and $\Phi = \Theta - \Psi$ can be introduced, as shown in Ref. [28], with which the macroscopic evolution equations can be expressed as follows:

$$\begin{aligned}\dot{x}(t) &= -y + (1-x^2)h + xyg,\\ \dot{y}(t) &= x - (1-y^2)g - xyh,\\ \dot{\Phi}(t) &= 1 - \frac{1}{1+\sqrt{1-x^2-y^2}}(xg+yh).\end{aligned} \tag{18}$$

Hereafter, we refer to the sets of three macroscopic variables, i.e., (γ,Θ,Ψ) or (x,y,Φ), as the WS variables.

To specify the system state, we need to fix $N+3$ constants, namely, the N constants of motion $\{\psi_j\}$ and three initial conditions $\gamma(0)$, $\Theta(0)$, and $\Psi(0)$ for the macroscopic variables. Because the original system is N dimensional, we need to restrict the three excess degrees of freedom by imposing three constraints as explained in Ref. [28]. We use the simplest rule for converting the initial phases $\{\theta_j(0)\}$ to the constants of motion $\{\psi_j\}$ and to the WS variables [28],

$$\gamma(0) = 0, \quad \Theta(0) = 0, \quad \Psi(0) = 0, \quad \{\psi_j = \theta_j(0)\} \tag{19}$$

or equivalently,

$$x(0) = 0, \quad y(0) = 0, \quad \Phi(0) = 0, \quad \{\psi_j = \theta_j(0)\}, \tag{20}$$

where $j = 1,\ldots,N$. With this choice, the WS variables always start from the origin while their dynamics (governing equations) changes depending on the initial phase distribution $\{\theta_j\}$ through the functions g and h.

VI. DYNAMICS OF THE WATANABE-STROGATZ VARIABLES

Using the three WS transformations, we can visualize the trajectories of the system in a space of (γ,Θ,Ψ) or (x,y,Φ), which obey the reduced evolution equation (14) or (18) equivalent to the original equation (2). We use $N = 20$ oscillators, whose initial phases are selected randomly from $[0,2\pi)$. The numerical simulations of both the original and reduced WS equations yield the same results. Figure 8 shows the dynamics of the WS variables, which corresponds to Fig. 1 with random initial conditions. The WS variables (x,y,Φ) are plotted in Figs. 8(a), 8(c), and 8(e) using cylindrical polar coordinates, and in Figs. 8(b), 8(d), and 8(f) by projecting them onto the x-y plane.

Correspondence between the three dynamical states of the original system and the dynamics of the WS equation is given in Refs. [27–30]. The synchronization rate R and the WS variable $\gamma = \sqrt{x^2+y^2}$ are qualitatively similar in the sense that $\gamma = 0$ when $R = 0$ and $\gamma = 1$ when $R = 1$, though they are not equal when $0 < R$ and $\gamma < 1$. The locked state corresponds to a fixed point of the WS equation with $\gamma = 1$, $\Theta = \bar{\theta} + \pi$, and arbitrary Ψ (hence $\Phi = \Theta - \Phi$). The synchronized drifting state corresponds to a fully circular closed orbit of radius $\gamma = 1$ on the x-y plane. The variable Θ

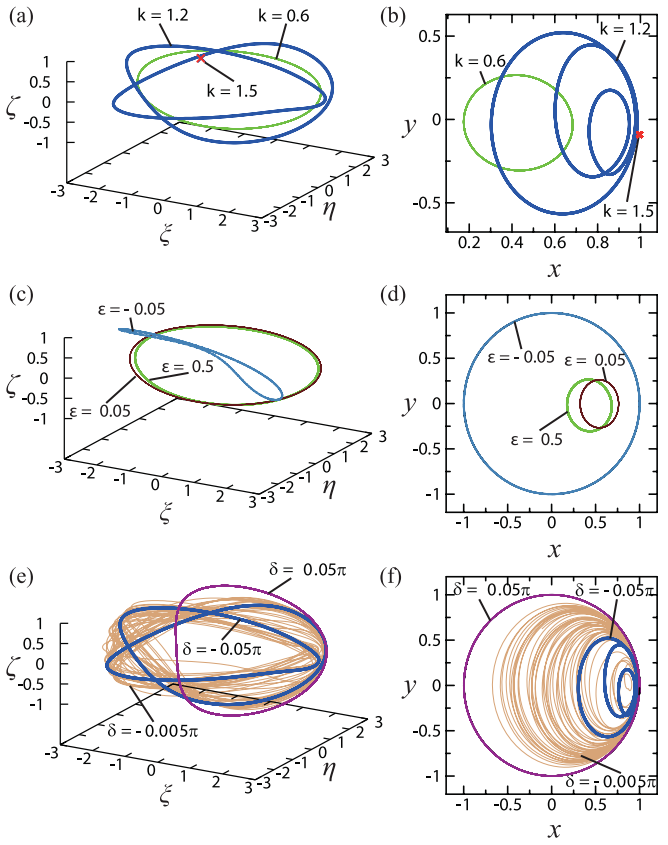

FIG. 8. (Color online) Trajectories of the WS variables evolving under Eq. (18), which correspond to Fig. 1. The number of oscillators is $N = 20$. Initial phases are selected randomly from a uniform distribution in $[0,2\pi)$. In (a), (c), and (e), the trajectories are plotted on a torus using cylindrical polar coordinates $\xi = (x+2)\cos\Phi$, $\eta = (x+2)\sin\Phi$, and $\zeta = y$, where $\Psi = 0$ and $\Psi = 2\pi$ are connected. In (b), (d), and (f), the trajectories are projected on the x-y plane. (a),(b) External forcing intensity k is varied while the coupling strength $\epsilon = 0.5$ and the coupling phase shift $\delta = -0.05\pi$ are fixed. (c),(d) ϵ is varied while $k = 0.6$ and $\delta = -0.05\pi$ are fixed. (e),(f) δ is varied while $k = 1.2$ and $\epsilon = 0.5$ are fixed.

decreases (Φ increases) and Ψ can take an arbitrary constant. The asynchronous state without fluctuations corresponds to a fixed point in the x-y plane with $0 < \gamma < 1$, while $\Phi = \Theta - \Psi$ increases. The asynchronous state with periodic (chaotic) fluctuations corresponds to a limit cycle (chaotic orbit) in the WS phase space.

Figures 8(a) and 8(b) plot the trajectories of the WS variables at $k = 0.6$, $k = 1.2$, or $k = 1.5$ with $\epsilon = 0.5$ and $\delta = -0.05\pi$. At $k = 1.5$, the system is in the locked state and $R = 1$. Correspondingly, the WS variables converge to a fixed point with $\gamma = 1$. At $k = 0.6$ or $k = 1.2$, the system is in the asynchronous fluctuating state. The WS variables go around a closed limit-cycle orbit, whose radius $\gamma < 1$ and whose shape depends on k. We observe that the periodic fluctuations in R at $k = 0.6$ and $k = 1.2$ shown in Figs. 1(a) and 1(b) correspond to limit cycles of the WS variables, and the constant R at $k = 1.5$ corresponds to a fixed point of the WS variables. Therefore persistent fluctuations in the synchronization rate are in fact collective low-dimensional dynamics in the high-dimensional phase space of coupled oscillators.

Similarly, Figs. 8(c) and 8(d) plot the WS variables at $\epsilon = 0.5$, 0.05, and -0.05, while keeping $k = 0.6$ and $\delta = -0.05\pi$ fixed. When $\epsilon < 0$, the coupling is attractive and the system converges to the synchronized drifting state with $R = 1$. The corresponding WS trajectory is a full circle on the x-y plane with $\gamma = 1$; the trajectory becomes distorted when it is plotted in cylindrical coordinates. When $\epsilon > 0$, the coupling is repulsive and the system is in the asynchronous fluctuating state. The WS trajectory contracts to a small, closed circular orbit on the x-y plane with γ smaller than 1, which correspond to a closed orbit along the longitude of the cylinder.

Finally, Figs. 8(e) and 8(f) show the dynamics of the WS variables at $\delta = -0.05\pi$, $\delta = -0.005\pi$, and $\delta = 0.05\pi$, which corresponding to Figs. 1(e) and 1(f). $k = 1.2$ and $\epsilon = 0.5$ are fixed. When $\delta = 0.05\pi$, the system is in the synchronized drifting state with $R = 1$ and the WS variables approach a full circle on the x-y plane with $\gamma = 1$. When $\delta = -0.05\pi$, the synchronization rate fluctuates periodically and the WS variables form a smaller limit cycle with $\gamma < 1$. For the chaotic fluctuations observed in the synchronization rate at $\delta = -0.005\pi$, the corresponding WS orbit is also chaotic.

VII. INHOMOGENEITY OF INITIAL CONDITIONS AND THE FINITE-SIZE EFFECTS

In the previous section, we observed that the fluctuations in the synchronization rate corresponded to low-dimensional periodic or chaotic dynamics of the reduced WS equations. Here, to explain the dependence of ΔR on N, we analyze the WS dynamics perturbatively near the splay state within the limit of large N.

A. Splay-state initial condition

From the conversion rule Eq. (19), the splay-state initial conditions for the oscillators $\theta_j(0) = 2\pi j/N$ are mapped to the constants of motion $\psi_j = 2\pi j/N$. Therefore, in the continuum limit $N \to \infty$, the functions P and Q in Eq. (16) can be approximated by integrals as

$$\begin{aligned} P_0 &= \frac{1}{2\pi}\int_0^{2\pi} F(\psi - \Psi)d\psi = \frac{\gamma}{1+\sqrt{1-\gamma^2}} \\ &= \frac{\sqrt{x^2+y^2}}{1+\sqrt{1-x^2-y^2}}, \\ Q_0 &= \frac{1}{2\pi}\int_0^{2\pi} G(\psi - \Psi)d\psi = 0. \end{aligned} \tag{21}$$

Therefore the dependence of P and Q on Φ vanishes, and the functions g and h in Eq. (15) are given as

$$\begin{aligned} g_0 &= -\epsilon\frac{1-\sqrt{1-\gamma^2}}{\gamma}\cos(\Theta - \delta) + k \\ &= -\frac{\epsilon}{1+\sqrt{1-x^2-y^2}}(x\cos\delta + y\sin\delta) + k, \\ h_0 &= -\epsilon\frac{1-\sqrt{1-\gamma^2}}{\gamma}\sin(\Theta - \delta) \\ &= -\frac{\epsilon}{1+\sqrt{1-x^2-y^2}}(-x\sin\delta + y\cos\delta). \end{aligned} \tag{22}$$

These relations and Eq. (18) indicate that in the $N \to \infty$ limit, the WS equations can be written in the form

$$\dot{x}(t) = U_0(x,y), \quad \dot{y}(t) = V_0(x,y), \quad \dot{\Phi}(t) = W_0(x,y), \quad (23)$$

where the vector field (U_0, V_0, W_0) is given from Eqs. (18) and (22) as

$$\begin{aligned} U_0(x,y) &= -y + (1-x^2)h_0 + xyg_0, \\ V_0(x,y) &= x - (1-y^2)g_0 - xyh_0, \\ W_0(x,y) &= 1 - \frac{1}{1+\sqrt{1-x^2-y^2}}(xg_0 + yh_0). \end{aligned} \quad (24)$$

It should be noted that all U_0, V_0, W_0 depend only on (x,y), and thus Φ is passively driven by x and y. Therefore the dynamics is essentially closed within the two dynamical variables (x,y) when the system starts from the splay state [27,28]. The numerical analysis of this two-dimensional system indicate that (x,y) settles to a stable fixed point (x_0,y_0) satisfying $U_0(x_0,y_0) = 0$ and $V_0(x_0,y_0) = 0$, which generally depends on ϵ, δ, and k. Correspondingly, the variable Φ constantly increases as $\Phi(t) = \beta t$, where β is given by $\beta = W_0(x_0,y_0)$. Although it is difficult to obtain (x_0,y_0) analytically, on the basis of numerical results, we assume that (x_0,y_0) remains linearly stable and (x,y) does not exhibit oscillations if the parameters are varied in the asynchronous state.

B. Effect of initial inhomogeneity

Now, we consider slightly perturbed initial conditions from the splay state, $\theta_j(0) = 2\pi j/N$. We shift the initial phase of each oscillator $\theta_j(0)$, which is equal to the constant ψ_j, by a small amount μa_j $(j = 1, \ldots, N)$. Here, a_j is an arbitrary constant of $O(1)$, and μ is a parameter that is introduced to represent smallness of the inhomogeneity. The first-order correction to P and Q can be estimated in the $N, M \to \infty$ limit by expanding F and G as

$$\begin{aligned} P &= \frac{1}{N}\sum_{j=1}^{N} F(\psi_j + \mu a_j - \Psi) \\ &= \frac{1}{N}\sum_{j=1}^{N} F(\psi_j - \Psi) + \mu\frac{1}{N}\sum_{j=1}^{N} a_j F'(\psi_j - \Psi) + O(\mu^2) \\ &\approx \frac{1}{2\pi}\int_0^{2\pi} F(\psi - \Psi)d\psi \\ &\quad + \mu\frac{1}{2\pi}\int_0^{2\pi} F'(\psi - \Psi)a(\psi)d\psi + O(\mu^2) \end{aligned} \quad (25)$$

and similarly

$$\begin{aligned} Q &= \frac{1}{N}\sum_{j=1}^{N} G(\psi_j + \mu a_j - \Psi) \\ &= \frac{1}{N}\sum_{j=1}^{N} G(\psi_j - \Psi) + \mu\frac{1}{N}\sum_{j=1}^{N} a_j G'(\psi_j - \Psi) + O(\mu^2) \\ &\approx \frac{1}{2\pi}\int_0^{2\pi} G(\psi - \Psi)d\psi \\ &\quad + \mu\frac{1}{2\pi}\int_0^{2\pi} G'(\psi - \Psi)a(\psi)d\psi + O(\mu^2). \end{aligned} \quad (26)$$

Therefore, for small μ, P and Q can be approximated as

$$P = P_0 + \mu P_1, \quad Q = Q_0 + \mu Q_1, \quad (27)$$

where P_1 and Q_1 are given by

$$\begin{aligned} P_1 &\approx \frac{1}{2\pi}\int_0^{2\pi} F'(\psi - \Psi)a(\psi)d\psi, \\ Q_1 &\approx \frac{1}{2\pi}\int_0^{2\pi} G'(\psi - \Psi)a(\psi)d\psi, \end{aligned} \quad (28)$$

and, correspondingly, the functions g and h can be expressed as

$$g = g_0 + \mu g_1, \quad h = h_0 + \mu h_1. \quad (29)$$

In contrast to P_0 and Q_0 (and therefore g_0 and h_0), P_1 and Q_1 (g_1 and h_1) depend on Φ through $\Psi = \Theta - \Phi$. Therefore from Eq. (18), the approximated WS equations can be written in the form

$$\begin{aligned} \dot{x}(t) &= U_0(x,y) + \mu U_1(x,y,\Phi), \\ \dot{y}(t) &= V_0(x,y) + \mu V_1(x,y,\Phi), \\ \dot{\Phi}(t) &= W_0(x,y) + \mu W_1(x,y,\Phi). \end{aligned} \quad (30)$$

That is, by shifting the initial conditions slightly from the splay state, feedback terms of $O(\mu)$ from Φ to (x,y) arise. It is expected that the perturbation terms result in periodic (or chaotic) fluctuations of $O(\mu)$ in (x,y).

To observe this more explicitly, we expand $x(t)$, $y(t)$, and $\Phi(t)$ around the unperturbed solutions $x(t) = x_0$, $y(t) = y_0$, and $\Phi(t) = \beta t$, respectively, in series of μ as

$$\begin{aligned} x(t) &= x_0 + \mu x_1(t) + O(\mu^2), \\ y(t) &= y_0 + \mu y_1(t) + O(\mu^2), \\ \Phi(t) &= \beta t + \mu\Phi_1(t) + O(\mu^2), \end{aligned} \quad (31)$$

and substitute them into Eq. (30). At the first order $O(\mu)$, we obtain

$$\begin{aligned} \dot{x}_1(t) &= \left(\frac{\partial U_0}{\partial x}x_1 + \frac{\partial U_0}{\partial y}y_1\right) + U_1(x_0,y_0,\beta t), \\ \dot{y}_1(t) &= \left(\frac{\partial V_0}{\partial x}x_1 + \frac{\partial V_0}{\partial y}y_1\right) + V_1(x_0,y_0,\beta t), \\ \dot{\Phi}_1(t) &= \left(\frac{\partial W_0}{\partial x}x_1 + \frac{\partial W_0}{\partial y}y_1\right) + W_1(x_0,y_0,\beta t), \end{aligned} \quad (32)$$

where partial derivatives are estimated at $(x,y) = (x_0,y_0)$. It should be noted that the Jacobian matrix J of the fixed point (x_0,y_0) appears in the equations for (x_1,y_1). Numerical analysis shows that the fixed point (x_0,y_0) is linearly stable, i.e., the eigenvalues of the Jacobian have negative real parts, and the deviation (x_1,y_1) from the fixed point tends to decay exponentially. However, the inhomogeneous periodic forcing terms U_1 and V_1 drive (x_1,y_1) away from zero with frequency β [the solution sufficiently after the initial transient is given as $(x_1(t),y_1(t))^T = \int_{-\infty}^{t} e^{(t-s)J}(U_1(s),V_1(s))^T ds$]. Therefore, from Eq. (31), the fluctuations of $O(\mu)$ around (x_0,y_0) due to the feedback from the Φ component is expected.

C. Isolated inhomogeneity at the origin

As an example, we shift the initial phases of the first $M = \rho N$ oscillators from $j = 1$ to M by a constant a from the splay

state and take the $N, M \to \infty$ limit while keeping their ratio $0 \leqslant \rho \ll 1$ fixed. This limit corresponds to the continuum limit of the slightly perturbed splay-state initial conditions that we considered in Sec. III. In this limit, we have $a(\psi) = a$ for $0 \leqslant \psi < 2\pi\rho$ and $a(\psi) = 0$ for $2\pi\rho \leqslant \psi < 2\pi$, so the integrals in Eq. (28) can be approximated as

$$\begin{aligned} \frac{1}{2\pi}\int_0^{2\pi\rho} aF'(\psi-\Psi)d\psi &\approx a\rho F'(-\Psi), \\ \frac{1}{2\pi}\int_0^{2\pi\rho} aG'(\psi-\Psi)d\psi &\approx a\rho G'(-\Psi), \end{aligned} \tag{33}$$

and thus P_1 and Q_1 are explicitly calculated as

$$\begin{aligned} P_1 &= a\rho\frac{(1-\gamma^2)\sin\Psi}{(\gamma\cos\Psi-1)^2}, \\ Q_1 &= a\rho\frac{\sqrt{1-\gamma^2}(\cos\Psi-\gamma)}{(\gamma\cos\Psi-1)^2}, \end{aligned} \tag{34}$$

which may also be expressed as functions of x, y, and Φ. It is clear that the combination $a\rho$ measures the degree of inhomogeneity from the splay state.

In Fig. 9(a), the numerical simulations of the original system (2), equivalent WS equation (18), and approximated WS equation in the continuum limit given by Eqs. (30) and (34) are compared for slightly perturbed splay-state initial conditions. The number of the oscillators is $N = 100$ and only a single oscillator ($M = 1$) is shifted, which gives $\rho = M/N = 1/100 = 0.01$. The formal expansion parameter μ is set to 1, and the small phase shift is set to be $a = 0.1$. We observe that the result of the approximated WS equation in the continuum limit agrees well with the results of the original system and the equivalent WS equation. The approximation is generally accurate in a wide parameter region in the asynchronous state as long as a is small, though deviations from the direct numerical simulation of the original model can be enhanced near the border between the asynchronous state and the locked or synchronized drifting state. Further, it should be noted also that chaos never occurs within this first-order approximation.

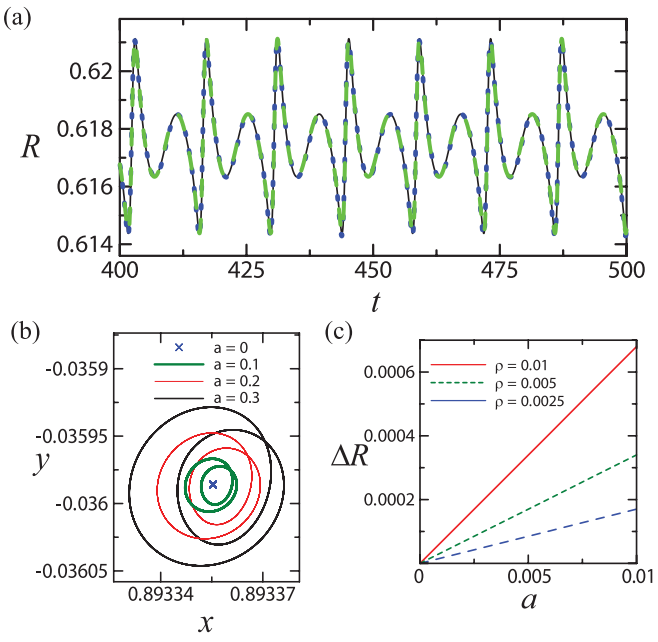

FIG. 9. (Color online) (a) Time sequences of the synchronization rate R obtained by numerical simulations of the original equation (solid black curve), the WS equations with a finite number of $N = 100$ (dashed green curve), and the approximated WS equations in the continuum limit (blue dotted curve). The initial shift is $a = 0.1$ and the proportion of the shifted oscillator is $\rho = M/N = 1/100 = 0.01$. (b) Trajectories of the approximated WS equations in the continuum limit on the x-y plane for differing values of a and fixed $\rho = 0.01$. (c) Amplitude of the fluctuations ΔR vs the small parameter $a\rho$ obtained numerically from the approximated WS equations in the continuum limit for differing values of a and fixed $\rho = 0.01$, $\rho = 0.005$, and $\rho = 0.0025$. The parameter values are $\epsilon = 0.5$, $k = 1.2$, and $\delta = -0.05\pi$.

In Fig. 9(b), typical solutions of the approximated WS equation in the continuum limit are plotted, where the degree of the inhomogeneity $a\rho$ is varied as the control parameter. We observe that the trajectories on the x-y plane have almost the same shape and only their size becomes larger as a is increased. In fact, the size is proportional to $a\rho$, as expected from the perturbation analysis given above. Figure 9(c) plots ΔR calculated from the approximated WS equation. It is clear that ΔR depends approximately linearly on $a\rho$. In other words, the amplitude of fluctuations in the synchronization rate is controlled by the degree of inhomogeneity added to the splay state in the initial phase distribution.

The above results elucidate the dependence of ΔR on N for the slightly shifted initial conditions that we determined in Sec. III. When only a single oscillator at the origin is shifted from the splay state ($M = 1$) and N is increased, we have $a\rho = aM/N$ and thus ΔR is inversely proportional to N. In contrast, if the proportion $\rho = M/N$ of the shifted oscillator is fixed, the degree of inhomogeneity $a\rho = aM/N$ is also kept constant and thus ΔR remains at the same order even if N is varied.

D. Random initial conditions

The dependence of ΔR on N for random initial conditions can be argued similarly. The functions P and Q in Eq. (16) can be considered sample averages over a finite number of the random variables $\{\psi_j\}$ ($j = 1, \ldots, N$) drawn from a uniform distribution in $[0, 2\pi)$, which we denote by P_N and Q_N. Their continuum limits P_0 and Q_0 in Eq. (21) can also be interpreted as ensemble averages $\langle P\rangle$ and $\langle Q\rangle$ with respect to a uniform distribution $p(\psi) = 1/2\pi$ of the random variable ψ. Therefore we can estimate the degree of deviations of the sample averages P_N and Q_N from the true ensemble averages $\langle P\rangle$ and $\langle Q\rangle$. Usually, the variances $\langle(P_N - \langle P\rangle)^2\rangle$ and $\langle(Q_N - \langle Q\rangle)^2\rangle$ are proportional to $1/N$ if the random variable ψ is selected independently. Therefore the inhomogeneity of the initial conditions scales as $1/\sqrt{N}$ for the random initial conditions. Taking into account the previous results for the shift of the initial conditions, which suggest that ΔR is approximately proportional to the degree of inhomogeneity given to the splay state, we expect that ΔR for the system with random initial conditions scales as $1/\sqrt{N}$.

Figure 10 shows the dependence of $\langle\Delta R\rangle$ on N for the random initial conditions. Here, $\langle\Delta R\rangle$ is averaged over 30 different random initial conditions. We can clearly observe

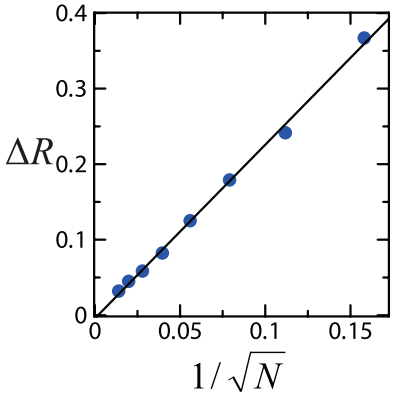

FIG. 10. (Color online) Dependence of the synchronization rate R and the amplitude of fluctuations ΔR on the number of oscillators N for systems started from random initial conditions. Averaged amplitude ΔR over 30 trials is plotted as a function of $1/\sqrt{N}$. The solid line indicates a linear regression. The parameter values are $k = 1.2$, $\epsilon = 0.5$, and $\delta = -0.05\pi$.

that $\langle \Delta R \rangle$ scales as $1/\sqrt{N}$. This confirms our interpretation of the numerical simulations in Sec. III, which indicate that the fluctuations in the synchronization rate are caused by the inhomogeneity (deviations from the splay state) due to the finiteness of the number of oscillators.

VIII. SUMMARY

We studied a system of phase oscillators with global coupling and periodic external forcing. In the asynchronous state of the system, typically periodic (sometimes chaotic) fluctuations in the synchronization rate are observed; these fluctuations strongly depend on the initial configurations of the phase oscillators. The fluctuations in the synchronization rate correspond to the limit-cycle (or chaotic) trajectories of the macroscopic Watanabe-Strogatz variables, i.e., they are deterministic low-dimensional collective dynamics of the system. The amplitude of the fluctuations in the synchronization rate is essentially determined by the degree of inhomogeneity of the initial conditions of the oscillators, i.e., their deviations from the splay state. The dependence of the amplitude of fluctuations on the number of oscillators for random initial conditions can also be interpreted similarly.

The fluctuations in the synchronization rate are reminiscent of those in the mean field in globally coupled chaotic maps [31–33]. In the case of globally coupled chaotic maps, owing to small correlations that remain among the chaotic maps even in the asynchronous regime, the mean field fluctuations do not decay to zero even if the number of chaotic maps N is increased. The main difference in the present case from the globally coupled maps is that the fluctuations are due to the existence of the constants of motion and therefore depend strongly on initial conditions. By virtue of the Watanabe-Strogatz ansatz, the system can directly be reduced to three macroscopic variables and the fluctuations can be traced back to the initial inhomogeneity. However, it is interesting to note that the perturbative approach to the fluctuations in the WS variables that we used in the present study somehow resembles the linear-response approach to the Frobenius-Perron equation describing the globally coupled maps [32,33].

Our results indicate that the dynamics in the asynchronous state of the system can differ significantly depending on initial phase distributions. This is in contrast to the locked or synchronized drifting states, in which the system settles to the same simple dynamics irrespective of the initial conditions. This observation may be relevant in understanding systems consisting of dynamical elements exhibiting nonstationary fluctuations.

ACKNOWLEDGMENTS

We thank S. Watanabe, H. Daido, T. Aoki, and H. Chiba for their useful comments. H.N. appreciates the financial support provided by KAKENHI (22684020) from MEXT, the CREST Kokubu Project from JST, and the Aihara Project, the FIRST program from JSPS, initiated by the Council for Science and Technology Policy, Japan.

[1] J. L. Van Hemmen and W. F. Wreszinski, J. Stat. Phys. **72**, 145 (1993).
[2] J. A. Acebron, L. L. Bonilla, C. J. Perez Vicente, F. Ritort, and R. Spigler, Rev. Mod. Phys. **77**, 137 (2005).
[3] R. E. Mirollo and S. H. Strogatz, SIAM J. Appl. Math. **50**, 1645 (1990).
[4] K. Okuda, Physica D **63**, 424 (1993).
[5] D. Golomb, D. Hansel, B. Shraiman, and H. Sompolinsky, Phys. Rev. A **45**, 3516 (1992).
[6] D. Hansel, G. Mato, and C. Meunier, Phys. Rev. E **48**, 3470 (1993).
[7] H. Kori and Y. Kuramoto, Phys. Rev. E **63**, 046214 (2001).
[8] V. Hakim and W.-J. Rappel, Phys. Rev. A **46**, R7347 (1992).
[9] N. Nakagawa and Y. Kuramoto, Prog. Theor. Phys. **89**, 313 (1993).
[10] S. K. Han, C. Kurrer, and Y. Kuramoto, Phys. Rev. Lett. **75**, 3190 (1995).
[11] M. Tachikawa and K. Fujimoto, Europhys. Lett. **78**, 20004 (2007).
[12] T.-W. Ko and G. B. Ermentrout, Phys. Rev. E **78**, 016203 (2008).
[13] H. Nakao and A. S. Mikhailov, Phys. Rev. E **79**, 036214 (2009).
[14] J. Buck and E. Buck, Sci. Am. **234**(5), 74 (1976).
[15] G. Buzsaki and A. Draguhn, Science **304**, 1926 (2004).
[16] H. Fukuda, N. Nakamichi, M. Hisatsune, H. Murase, and T. Mizuno, Phys. Rev. Lett. **99**, 098102 (2007).
[17] R. Hosoda, K. Nakayama, M. Kato-Negishi, M. Kawahara, K. Muramoto, and Y. Kuroda, Cell. Mol. Neurobiol. **23**, 895 (2003).
[18] Z. Neda, E. Ravasz, Y. Brechet, T. Vicsek, and A. L. Barabasi, Nature (London) **403**, 849 (2000).
[19] F. De Smet and D. Aeyels, Physica D **234**, 81 (2007).
[20] K. Wiesenfeld, P. Colet, and S. H. Strogatz, Phys. Rev. E **57**, 1563 (1998).
[21] H. Sakaguchi, Prog. Theor. Phys. **79**, 39 (1988).

[22] L. M. Childs and S. H. Strogatz, Chaos **18**, 043128 (2008).
[23] E. Ott and T. M. Antonsen, Chaos **19**, 023117 (2009); **18**, 037113 (2008).
[24] K. Agladze, M. W. Kay, V. Krinsky, and N. Sarvazyan, Am. J. Physiol. Heart Circ. Physiol. **293**, H503 (2007).
[25] C. Hammond, H. Bergman, and P. Brown, Trends Neurosci. **30**, 357 (2007).
[26] A. Pikovsky, M. Rosenblum, and J. Kurths, *Synchronization: A Universal Concept in Nonlinear Sciences* (Cambridge University Press, Cambridge, England, 2003).
[27] S. Watanabe and S. H. Strogatz, Phys. Rev. Lett. **70**, 2391 (1993).
[28] S. Watanabe and S. H. Strogatz, Physica D **74**, 197 (1994).
[29] A. Pikovsky and M. Rosenblum, Phys. Rev. Lett. **101**, 264103 (2008).
[30] S. A. Marvel, R. E. Mirollo, and S. H. Strogatz, Chaos **19**, 043104 (2009).
[31] K. Kaneko, Phys. Rev. Lett. **65**, 1391 (1990).
[32] T. Chawanya and S. Morita, Physica D **116**, 44 (1998).
[33] D. Topaj, W.-H. Kye, and A. Pikovsky, Phys. Rev. Lett. **87**, 074101 (2001).